Special Issue Article

JSA

J Strain Analysis
2014, Vol. 49(4) 233–243

DOI: 10.1177/0309324713503959
sdj.sagepub.com
SAGE

Digital image correlation study of mechanical response of nickel superalloy Hastelloy X under thermal and mechanical cycling: Uniaxial and biaxial stress states

Bharath Swaminathan[1,2], John Lambros[1] and Huseyin Sehitoglu[3]

Abstract

The cyclic plastic strain accumulation of a dynamic strain aging Ni-based superalloy, Hastelloy X, is investigated using digital image correlation under both uniaxial and biaxial thermomechanical loading conditions. Thermal cycling and uniaxial mechanical tensile loading demonstrate that this material exhibits a Cottrell–Stokes–type response in which yield stress is not fully recovered after a mechanical loading cycle followed by a second isothermal loading cycle at elevated temperature (between room temperature and 600 °C in this work). The Portevin–Le Chatelier dynamic strain aging effect at higher temperatures, which has been seen to occur in this material, may also contribute to this reduction in flow stress. Additionally, under biaxial stress states introduced by means of a double-notch experimental sample, various cyclic thermal and mechanical loading combinations demonstrated a complex thermomechanical plastic response of this material. For example, cyclic thermal loading experiments at fixed displacement amounts for each cycle show greater plastic strain accumulation after three cycles when cycling is performed at a combination of 300 °C and 600 °C than that for three isothermal 600 °C cycles.

Keywords

High temperature, notch, digital image correlation, Portevin–Le Chatelier effect, cyclic plasticity

Date received: 7 January 2013; accepted: 5 August 2013

Introduction

The demand for high-performance materials in structural applications for extreme environments has driven the development of new materials, such as superalloys, multifunctional composites, ceramics, and functionally graded materials. This necessitates the detailed understanding of the behavior of such materials, especially when there is a need to apply them to complex geometric and functional designs that are subject to diverse multiaxial loadings. In the case of metallic materials, it is also important to study their behavior in the plastic regime and uncover the underlying factors for their observed material response. An example of an extreme loading environment in the context of this work can be thought of as high-amplitude thermal and acoustic loads that, for example, would be present in a hypersonic flight vehicle.

In this work, Hastelloy X, a nickel-based superalloy, was chosen as a "simple" high-temperature alloy, with predictable behavior under isothermal and nonisothermal, cyclic thermomechanical loading.[1] However, the behavior of Hastelloy X is actually complex, as the hardening response under certain thermomechanical cycles was found to be unbounded by the isothermal behaviors at the same test temperatures.[2] In addition, chromium carbide precipitation in many Ni-based alloys can produce dynamic strain aging effects during deformation. For example, Jenkins and Smith[3] showed

[1]Aerospace Engineering, University of Illinois at Urbana-Champaign, Urbana, IL, USA
[2]Applied Materials, Inc., Sunnyvale, CA, USA
[3]Mechanical Science and Engineering, University of Illinois at Urbana-Champaign, Urbana, IL, USA

Corresponding author:
John Lambros, Aerospace Engineering, University of Illinois at Urbana-Champaign, 306 Talbot Laboratory, 104 South Wright St., Urbana, IL 61801, USA.
Email: lambros@illinois.edu

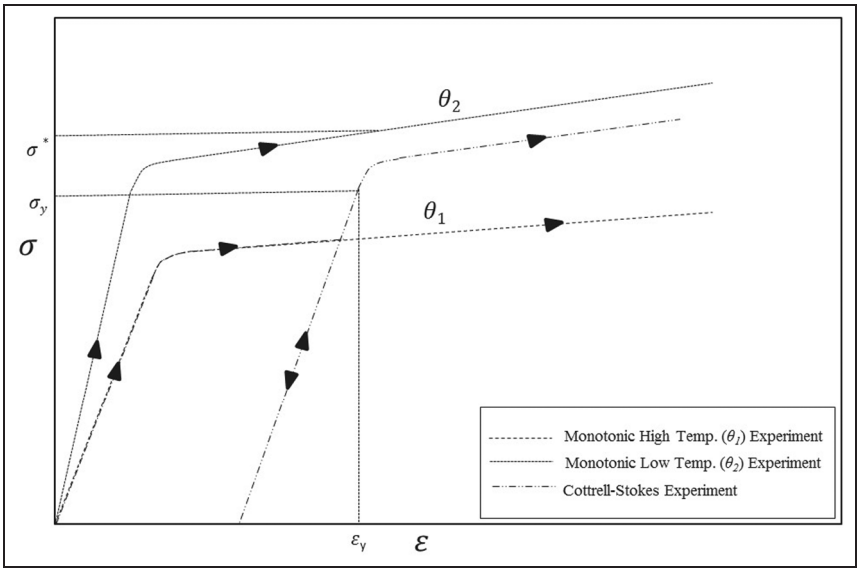

Figure 1. Schematic representation of the Cottrell–Stokes test[6] showing loading at two different temperatures ($\theta_2 < \theta_1$). Reloading after heating at θ_2 is shown with a corresponding drop in yield stress ($\sigma_y < \sigma^*$) from the isothermal level at a strain of ε_y.

that solute drag effects in Ni-based alloys below 300 °C were influenced by carbon alone. Sakthivel et al.[4] presented the stress–strain curves for Hastelloy X in the temperature range of 27–750 °C, at three different strain rates. They observed serrated flow at temperatures between 250 and 654 °C. Swaminathan et al.[5] also studied the serrated flow characteristics (Portevin–Le Chatelier (PLC) effect) in Hastelloy X using the optical technique of digital image correlation (DIC).

However, there are limited data available in the literature that characterize the response of Hastelloy X to *cyclic* thermal and mechanical loading. Such cyclic response, although most commonly modeled as an "additive superposition" of thermal and mechanical responses, can also often be quite complex. Cottrell and Stokes[6] using single crystals of aluminum showed that the tensile strength of materials deformed to a given strain at different temperatures depends on two parameters: (1) a reversible pure temperature dependence and (2) an irreversible change in the structure of the material. The irreversible change depends on the amount of strain and the temperature at which the straining takes place. Therefore, the tensile strength at a given temperature and strain is a function of both the temperature path and strain path to the final state. A "Cottrell–Stokes (CS) experiment" is one in which loading at high temperature is followed by unloading and reloading at a lower temperature. In many cases, such as that schematically illustrated in Figure 1, a drop in flow stress from the isothermal value upon reloading at the lower temperature is seen. An explanation of the yield drop based on theories of work hardening has been suggested in Kubin and Estrin.[7] The role of static and dynamic strain aging in the dislocation pile-up has also been studied by Kubin and Estrin.[8]

There is also experimental evidence to show that material inhomogeneity and geometric features affect the strain aging behavior of a material. The complexity of the material response under the effect of stress concentrations makes constitutive modeling a greater challenge, as was seen in the evolution of strain bands in specimens with U-notches.[9]

The need for accurate characterization of the mechanical behavior of materials at high temperatures has resulted in several studies at elevated temperatures, although not as widespread as studies at room temperatures (RTs), using full-field optical methods such as the optical metrology technique of DIC. Turner and Russell[10] studied the thermal expansion of aluminum, steel, and titanium using DIC with specimens that were prepared by spraying white manifold paint followed by a black speckle pattern. Coburn and Slevin[11] developed a laser speckle pattern to study the surface deformation of thermally stressed ceramics using DIC. Lyons et al.[12] conducted elevated temperature tests up to 650 °C to measure the thermal expansion of Incoloy 909 and study the deformation during uniform tensile loading, to demonstrate the effectiveness of DIC at high-temperature measurements. More recently, Pan et al.[13] carried out high-temperature image acquisition under blue light illumination.

The main objective of this work is to investigate the response of Hastelloy X, which is a high-performance Ni-based superalloy, under cyclic thermomechanical loading conditions, initially in the simpler case of uniaxial loading and subsequently under multiaxial stress states, which will be introduced by the presence of notches in the material. The specimen geometries used here are similar to those used in the studies of Tong et al.[9] and Benallal et al.[14] There have also been several recent studies that attribute flow stress variability to the presence of dynamic strain aging effects. Therefore, the specific objectives of this work are to (1) examine the material behavior under a CS test to investigate the

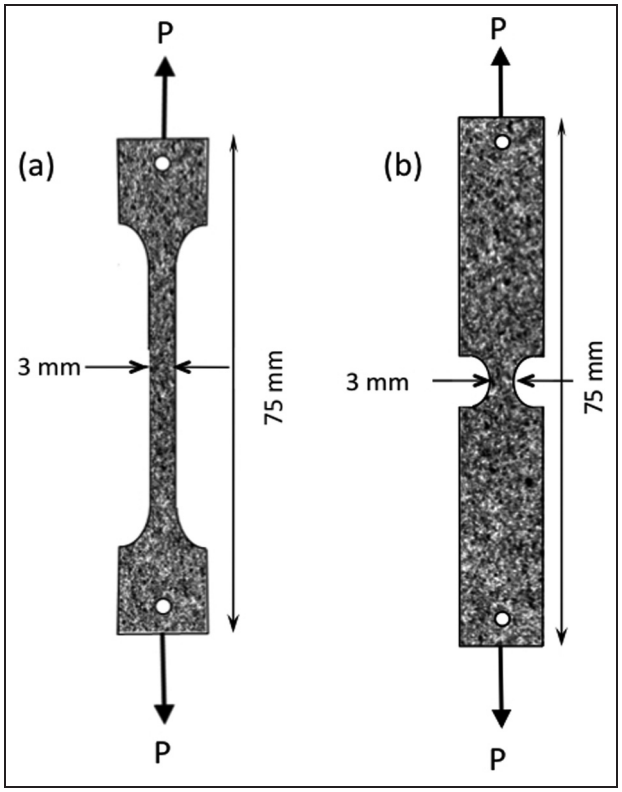

Figure 2. (a) Dog-bone specimen geometry and (b) double-U-notched specimen geometry. Both specimens have a nominal gauge section width of 3 mm and thickness of 1.5 mm. The notch radius is 1.5 mm.

influence of dynamic strain aging on the plastic history of Hastelloy X and (2) investigate the effect of stress concentrations on local plastic strain accumulation.

Experimental methods

Material and specimen preparation

The material used in this study was Hastelloy X, a solution heat-treated Nickel-based superalloy with superior high-temperature strength compared to conventional metals. All experiments in this study were conducted using specimens obtained from the same batch, and the specimens were cut so that loading in all cases would be applied parallel to the rolling direction of the plate. Two different loading configurations were used: (1) uniaxial tension using dog-bone-type specimens with far-field applied tensile displacements, as shown in Figure 2(a), and (2) a double-U-notched specimen geometry, as shown in Figure 2(b), which when subjected to uniaxial applied far-field loading will induce a biaxial stress state in the vicinity of the U-notches. Note that the holes shown at the top and bottom of the specimens in Figure 2 are only for alignment purposes and are not for loading pins. Gripping and loading was done with cooled hydraulic clamp-type grips with custom-built adapters to accommodate this particular specimen geometry.[15,16]

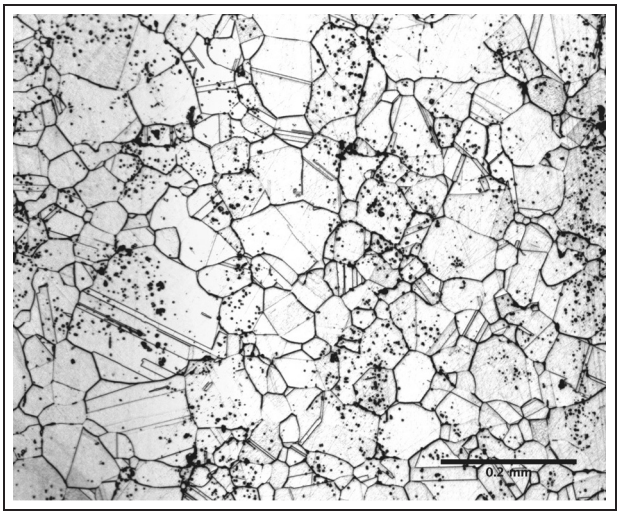

Figure 3. Grain structure of Hastelloy X, viewed under an optical microscope. The specimen was etched with Aqua regia. The corrosive nature of etchant is viewed as pitting marks on the surface and grain boundaries of the specimen. The average grain size was found to be about 60 μm, although most grains show annealing twins.

The specimens were machined in the geometries shown in Figure 2 using electro-discharge machining from a stock 3-mm-thick plate, which was cut in half in the through-thickness direction, to produce samples that were 1.5 mm thick. The overall specimen dimensions for both sample types are the same at 75 mm × 6 mm × 1.5 mm. The gauge section width for both sample types was 3 mm, while the gauge section length was 55 mm for the uniaxial tension samples, and the notch radius for the double-U-notched samples was 1.5 mm. The through-thickness sectioning process generated a newly exposed specimen surface. Both front and back specimen surfaces were polished with coarse grit (400, 600) followed by fine grit polishing papers (P1500, P 2400, and P4000), to ensure a flat surface for spraying a suitable speckle pattern. Figure 3 shows an optical micrograph of the grain structure of the Hastelloy X used, with the grain boundaries clearly revealed.

The average grain size was found to be about 60 μm, although, as seen in Figure 3, most grains show significant annealing twins, thus decreasing the effective grain size to about half this value. The 1.5-mm-thick samples used here imply that fewer number of grains (25 or so, up to 50 if we consider twins) may exist through the thickness compared to in-plane. This should not significantly alter the in-plane macroscopic measurements and observations made in this work, although local fields may be affected by the smaller number of through-thickness grains. In general, in the experimentation used here, which performed either far-field or surface measurements, little is known in the through-thickness direction where a plane stress assumption will be made. As eventually this type of Ni-based superalloy material is targeted for use in

high-temperature fatigue applications, the impact of the through-thickness grains is expected to be minor considering the significant experimental evidence showing fatigue cracks initiating at the surface.[16]

Loading and imaging

An Instron 8800 servo-hydraulic load frame was used to load the specimens, which were also heated, while their surface was imaged using a charge-coupled device (CCD) camera for subsequent use of DIC measurements. The process of DIC[17] is not detailed here, as it is a widely used technique that produces measurements of surface displacements and strains. Loading was controlled via a computer using a LabVIEW interface, which allowed control of the load ramp type as well as the magnitude and loading rate. There is also a provision for control of a CCD camera for capturing images in synchronization with the loading process. For experiments at elevated temperatures, an induction coil, connected to a LEPEL induction heater, was placed around the specimen. A chiller was used to circulate cooling water around the grips to prevent heating of the grip surfaces and maintain a constant grip temperature. This resulted in a temperature gradient in the specimen–grip interface. Since the induction coil spanned the entire gauge section of the specimen, there was a negligible spatial temperature gradient at the specimen location that was imaged. The specimen temperature was measured by welding a K-type (chromel/alumel) thermocouple to the unprepared surface of the specimen, which was directly behind the area that was imaged. In all tests, the temperature variation was limited to ± 5 °C of the nominal test temperature.

A Schott compact illuminator, fitted with a gooseneck fiber optic conduit, was used to provide uniform, high-intensity illumination to the specimen. The imaging setup consisted of an imiTech 8-bit 1920 $\times$ 1200 pixel CCD camera attached to a Navitar 12$\times$ zoom lens with a 2$\times$ adapter. Imaging was performed through the gaps, sized a few millimeter, in between the induction coils that were wrapped around the sample. A double-ramp LabVIEW program was used to load both the tension dog-bone and double-U-notched specimens on the load frame. Thermal loading was applied as quickly as the induction heater allowed, and for 600 °C peak temperature experiments, this translated to about a 90 s heating time. Thermal unloading was done in air simply by shutting off the induction heater and usually took comparable time to the thermal loading interval because of the relatively small sample size and the grip cooling used here. Mechanical loading commenced only after steady-state temperature was achieved in each case and was carried out in displacement control at a constant rate of 0.015 mm/s, while unloading was done in load control. In all experiments discussed here, the applied strain rate during the loading stage was kept at 10^{-4} s^{-1}. Unloading was performed over a 30-s period in each case, although load was controlled in order to avoid reverse (compressive) loading of the sample. Data from the load cell and linear variable differential transformer (LVDT) were also recorded by the LabVIEW program at a frequency of 20 Hz. Images were acquired from the program-controlled I-1394 FireWire camera at a rate of 0.5 frames per second (fps). Once the test was completed, the images were processed using a commercial DIC software Vic-2D.

The Vic-2D software obtains the displacement and strain components over the entire area and uses bi-cubic interpolation for sub-pixel resolution. The pixel spatial resolution achieved in these experiments with the optical system described above was 3.4 μm/pixel. A subset size of 51 $\times$ 51 pixels (173 $\times$ 173 μm^2) with an offset of 5 pixels was used to carry out the correlation, producing a total of about 30,000 correlation points of the area of interest, which was approximately a 3 mm $\times$ 3 mm field of view directly in the middle of each specimen. This subset size and offset were selected based on rigid motion tests to ensure good correlation between images and provide sufficient data points for analysis. The data were then visualized on Vic-2D and exported to MATLAB for further post-processing. Figure 6(d) shows an area of the specimen over which the DIC algorithm was used along with a surface speckle pattern.

Challenges with high-temperature DIC measurements

Despite prior efforts,[10–13] obtaining and imaging effective speckle patterns for high-temperature studies still remains a challenge. One challenge at higher temperatures is that the intensity of thermal radiation from the specimen can overwhelm the camera sensor, thus making it unable to capture the speckle pattern on the specimen surface. Another limitation of high-temperature DIC is possible damage to the speckle pattern itself at high temperatures. Powder-based paints undergo transition at higher temperatures, which causes a change in the speckle pattern with specimen deformation leading to failed or erroneous image correlation. Oxidation of the specimen surface is also a serious issue at higher temperatures, since it causes changes in the specimen surface roughness and affects the deformation behavior. In order to prevent oxidation of the prepared specimen surface, a coating of VHT® high-temperature white paint was sprayed onto the specimens using the procedure outlined by the paint supplier. The painted surface was then polished with fine grit polishing paper (P4000 grit) to ensure a smooth and even layer of paint.

A random speckle pattern was sprayed onto the painted surface using an Iwata Custom micron B airbrush. The paint media was VHT® high-temperature black paint. Once the speckle pattern was deposited, the specimens were heated up to the test temperature of 600 °C in an oven. This ensured that all the solvent

deposited during the speckling process was removed, and the paint particles were stabilized to avoid further reactions during the course of the experiment and ensure that the speckle pattern remained unchanged during the test.

Uniaxial tensile behavior of Hastelloy X under thermal cycling

In this study, experiments similar to those conducted by Cottrell and Stokes[6] on aluminum were carried out for Hastelloy X. The high- and low-temperature conditions were 600 °C and 27 °C (RT), respectively, and were chosen such that at the higher temperature, the material exhibits some strain hardening,[4,5] while the temporal thermal gradient was as high as the capability of the setup could allow. The temperature cycling was then reversed to observe the effect of plastic pre-hardening at a lower temperature followed by further loading in monotonic tension at a higher temperature.

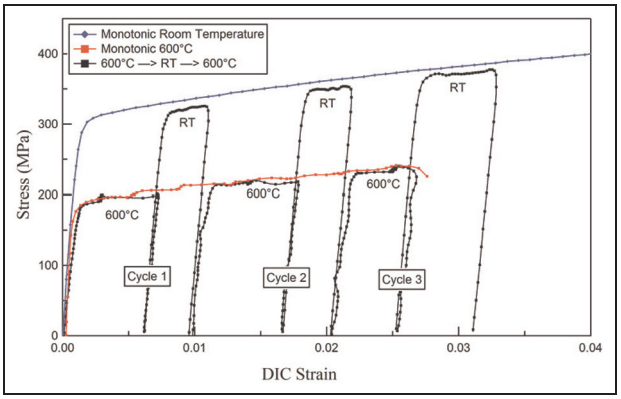

Figure 4. Cyclic Cottrell–Stokes response of Hastelloy X. Each RT cycle shows a drop in flow stress when compared to the monotonic response. The thermal strains were removed in the DIC analysis by comparing an image at RT with a subsequent image at 600 °C at no load and subtracting the mean strain from the strain data obtained for the high-temperature cycle.
DIC: digital image correlation; RT: room temperature.

CS-type experiment

The CS-type experiment was aimed at understanding the onset and evolution of plasticity following plastic work at a higher temperature. A dog-bone specimen was deformed at a higher temperature to a certain plastic strain and unloaded at the same temperature. The specimen was then air-cooled to RT, and the loading was continued till further plastic strain was accumulated. The same loading and unloading procedure was performed two more times for a total of three complete cycles—a single cycle being defined as loading at both the high and low temperatures. Before the start of mechanical loading at each cycle, the temperature was allowed to reach a steady-state value. Images were captured during both the high-temperature and low-temperature loading portions. The macroscopic tensile stress–strain response of Hastelloy X to the above-mentioned test protocol is presented in Figure 4, which shows the measured macroscopic stress plotted against the average strain recorded by the DIC method over the gauge length. The thermal component of strain has been removed between loading cycles. Isothermal curves at the two temperatures are also shown.

For the first CS loading–unloading–reloading cycle in Figure 4, the loading at high temperature follows the isothermal curve closely till the point of unloading with no observable difference in the flow stress or the yield point during this portion of loading. During this high-temperature portion, the PLC effect is clearly visible in the material response causing fluctuations in the stress–strain response, which are a result of the PLC effect and the temporal and spatial averaging process of DIC.[4,5] When the temperature is lowered to RT and the specimen is reloaded, the material yields at a *lower* stress than the nominal flow stress for the isothermal monotonic loading case. The material continues to strain with the same hardening rate, but does not reach the isothermal material flow stress upon further loading at that lower temperature. In the first loading–unloading–reloading cycle, the load drop is of the order of 20 MPa (~6% of the flow stress) and is comparable to the PLC serration amplitude seen at 600 °C. In the subsequent loading cycles, a similar effect is seen with the 600 °C portion of the loading generally agreeing with the isothermal monotonic stress–strain response, while the RT loading portions of the second and third cycles undershoot the isothermal flow stress by 24 (~6%) and 30 MPa (~8%), respectively.

Inverse CS-type experiment

An inverse test protocol was also carried out to determine the effect of plasticity at low temperature on the high-temperature flow behavior. The specimen was first loaded at RT and unloaded at a strain level between 2.5% and 3%. The temperature was then increased to 600 °C and allowed to reach steady state before further reloading. The process was then repeated for two additional loading–unloading–reloading cycles. The thermal strains were removed in the DIC analysis by comparing an image at RT with a subsequent image at 600 °C at no load and subtracting the mean strain from the strain data obtained for the high-temperature cycle. Following this fashion, only the net mechanical strain is plotted in Figure 5, which shows the comparison of the inverse CS test with the isothermal stress–strain curves at RT and 600 °C. During the first loading cycle at RT, the material responds as expected and follows the isothermal stress–strain curve. There is also good agreement during the first high-temperature cycle, the flow stress is very close to the flow stress under uniaxial monotonic tension and there is again evidence of

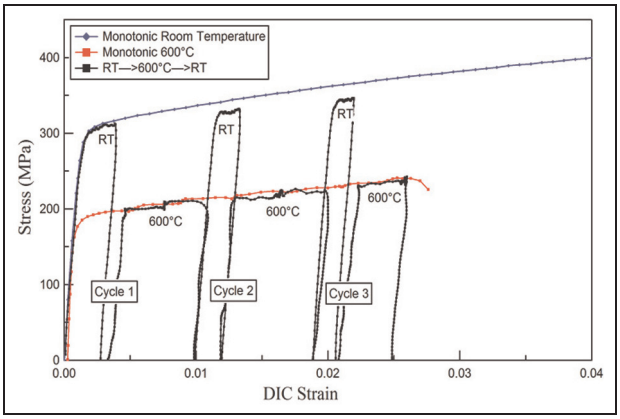

Figure 5. Inverse cyclic Cottrell–Stokes response of Hastelloy X. There is a drop in flow stress following the first high-temperature cycle, highlighting the effect of high-temperature plastic history on further plastic deformation.
DIC: digital image correlation; RT: room temperature.

serrated flow in the 600 °C cycle. However, in the second and third loading cycles at RT, the undershoot of flow stress from the isothermal case is again visible and in larger amounts than the CS-type case. The results here, which indicate that the PLC effect may influence path-dependent material response under thermal and mechanical cycling, point to the need of a refined constitutive model for Hastelloy X that would be capable of predicting this type of response. One such example is the generalized plasticity model of Sobotka and Dodds.[18]

Biaxial stress states under thermomechanical cycling

Most structural components possess some geometrical discontinuities that are necessitated by design to accommodate fasteners, joints, or weight reduction. There is a need to characterize localized plasticity in the presence of such discontinuities because of the stress concentration induced there. For a material like Hastelloy X that exhibits dynamic strain aging, the influence of combined thermal and mechanical loads at such stress concentration sites can also allow initiation of dynamic strain aging bands that may influence plasticity accumulation in the region. Hence, the local strain fields can be highly inhomogeneous in such biaxial, or in general triaxial, loading situations and may not be amenable to a predictive material model. The strain aging effect is studied in detail in Swaminathan et al.,[5] and although present in the experiments described here, as seen in Figures 4 and 5, is not the primary point of interest in this work. Rather, here we focus on the accumulation of plasticity under thermal and mechanical cycling in a multiaxial stress field in notched bars of Hastelloy X.

Machined double-notch specimens were used to carry out the experiments (Figure 2(b)), as they provided sufficient area for observation and imaging of the deformation between the two notches. As in the uniaxial loading case, cyclic plastic loading experiments were conducted at several temperature levels, either under isothermal conditions or with temperature jumps. A full-field measure of strain in the region around the notch can be obtained through the DIC measurements. Figure 6(a)–(c) shows the measured full-field strain components along the axial direction (direction of loading) and the transverse direction and the in-plane shear component, respectively, from a monotonic tension experiment of a double-notched sample at 600 °C. There is a strain concentration at each notch tip, which decreases as the center of the specimen between the two notches is approached. The strain fields are generally symmetric but do possess a large amount of local inhomogeneity. Note that the jagged edges around the notches in Figure 6(a)–(c), as well as the white speckles among the strain contours, are not representative of actual damage induced in the sample but are from locations where DIC has failed for some reason (either proximity to the boundary or pattern issues) and have not been indexed by Vic-2D.

To homogenize some of the significant strain inhomogeneities present, the average strain in a small region (a square of about 1.5 mm × 1.5 mm) between the two notches, highlighted in red Figure 6(d) and shown in the inset of Figure 7, was computed in order to study the samples' cyclic response. The region is selected such that it is centered about both the loading and notch axes. Figure 7(a) shows the axial strain history in this region for different temperatures. At RT, the response shows temporally smooth strain evolution, but at higher temperatures, jumps in strains are evidence of localized serrated plastic flow resulting from the PLC effect. At 300 °C, the strain jumps are more continuous, and of lower amplitude, than at 600 °C where the flow is interrupted by large jumps in between smaller strain jumps. Since all experiments were carried out under displacement control, the local strain jumps observed here are a consequence of global load drops due to specimen relaxation. Figure 7(b) and (c) shows the evolution of the transverse and the shear strain components in the same region shown in Figure 6(d), which also exhibit some nonuniform strain accumulation at higher temperatures.

The specimen was then subjected to multiple cycles at different temperatures under isothermal conditions—a cycle in this case refers to a single loading–unloading event. All experiments were performed under displacement control loading and load control unloading, and *the displacement applied during each cycle was kept constant at a level corresponding to 2.5% far-field strain*. Table 1 provides a summary of the thermal cycling experiments carried out on the double-U-notched specimens. The experiments with the 300°C–600 °C temperature cycles are dealt with in detail here. The lower temperature experiments do not show any deviation from expected

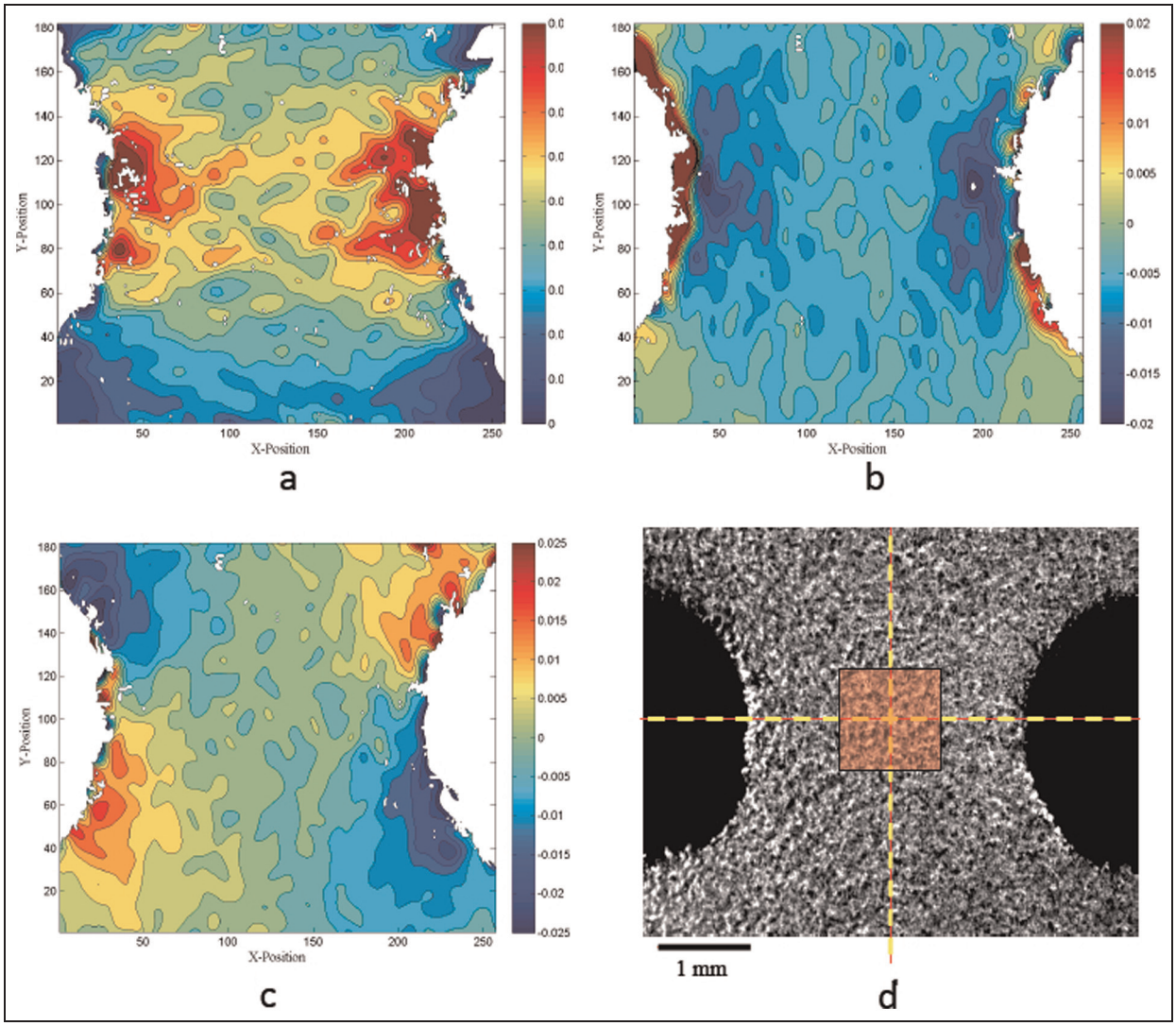

Figure 6. (a) Vertical strain (ε_{yy}) obtained from DIC analysis indicating an inhomogeneous strain field with stress concentration near the notch tip, (b) transverse strain (ε_{xx}), (c) shear strain (ε_{xy}), and (d) specimen with a speckle pattern indication window over which strain evolution is analyzed.

Table 1. Thermal cycling experiments with double-U-notched specimens.

Temperature range	Cycle 1	Cycle 2	Cycle 3
RT	RT	RT	RT
	RT	RT	300 °C
	RT	300 °C	RT
	300 °C	RT	RT
300 °C	300 °C	300 °C	300 °C
	300 °C	300 °C	600 °C
	300 °C	600 °C	300 °C
	600 °C	300 °C	300 °C
600 °C	600 °C	600 °C	600 °C

RT: room temperature.

behavior, as there is influence of strain hardening at lower temperatures.

Figure 8(a)–(c) shows the load–displacement curves for cyclic experiments with three loading cycles at 300 °C–300 °C–600 °C, 300 °C–600 °C–300 °C, and 600 °C–300 °C–300 °C, respectively. Figure 8(d) shows the curves for an isothermal 600°C–600°C–600°C three-cycle experiment. Although there is not much difference in the macroscale response, as will be seen subsequently, there is a large variation in the local behavior as measured by the DIC setup. The first comparison, presented in Figure 9, shows DIC contour plots of the final residual vertical strain at the end of three cycles from four specimens subjected to three loading cycles each at the following temperatures: (a) 600 °C–600 °C–600 °C, (b) 300 °C–300 °C–600 °C, (c) 300 °C–600 °C–300 °C, and (d) 600 °C–300 °C–300 °C. Figure 9(a) shows the strain field for the isothermal experiment with all three loading cycles conducted at 600 °C *after the specimen was unloaded* after the third cycle (i.e. in these plots the strain field comprised only the plastic strain component accumulated after all three cycles). The specimen with the two 300 °C cycles, Figure 9(b), shows *higher* final strains than the isothermal 600 °C specimen loaded in three cycles, even though yield stress at

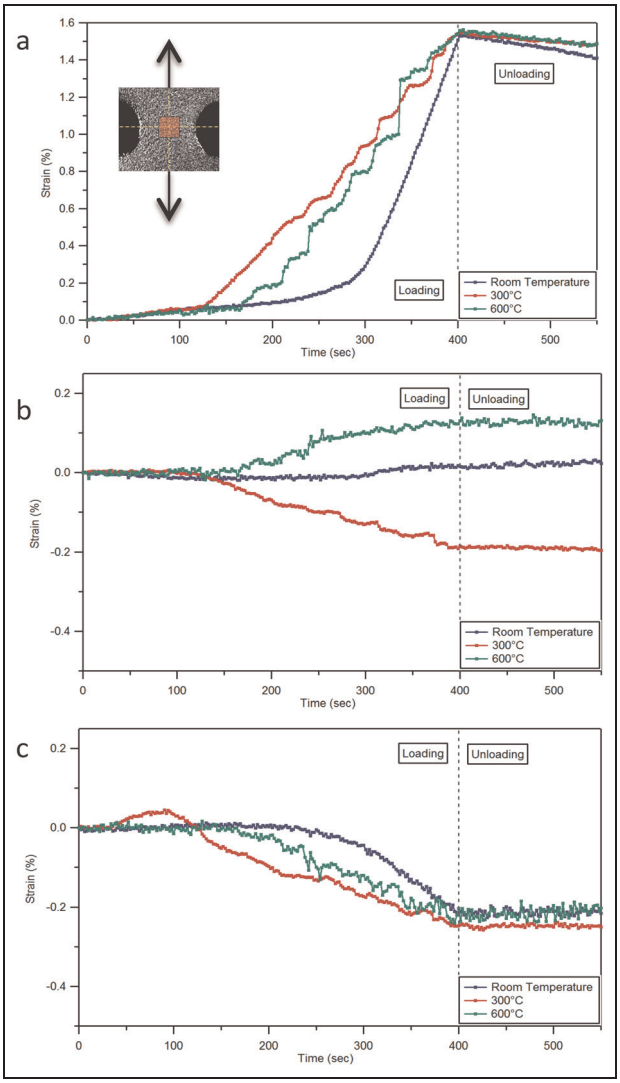

Figure 7. Average strain history over the region shown in the inset at different temperatures under the influence of the notches. There is evidence of dynamic strain aging at 300 °C and 600 °C: (a) axial strain along loading direction, (b) transverse strain, and (c) shear strain.

600 °C is lower. The occurrence of larger strain jumps seen at 300 °C in the monotonic dog-bone tension experiments with increasing plastic strains possibly explains the increased strain observed in Figure 9(b) over Figure 9(a). In contrast, at isothermal 600 °C conditions, the PLC effect is diminished at higher strains,[5] thus producing overall less strain accumulation.

The sequence of the 300 °C and 600 °C cycles also has an influence on the final plastic strain field achieved. It was observed that if high-temperature cycle occurs between or precedes the low-temperature cycles, then the final plastic strains obtained are lower than those in the isothermal case. (Recall that each loading cycle in all these experiments corresponds to the same amount of applied *displacement*.) Figure 9(c) shows the final residual strain field for the case of a specimen loaded with a 300 °C–600 °C–300 °C cycling, and Figure 9(d) shows that for the case of another specimen loaded with a 600 °C–300 °C–300 °C cycling. In both cases, the strains around the double notch are lower than the strain obtained in the isothermal experiment (Figure 9(a)). From these results, it appears that PLC strain bands are seen to start accumulating strain away from the centerline of the notch (note that in Figure 9(b)–(d) the maximum strains occur away from the centerline). This provides a new insight into stress concentration under load cycling in dynamic strain aging materials. Certainly, local microstructure also plays a role in accumulating plastic strains[19] and can lead to local inhomogeneities in strain. However, the strain band formation from the PLC phenomenon itself has been studied extensively in Swaminathan et al.,[5] and it is believed that it does contribute significantly to local strain inhomogeneity near the notches in addition to any microstructural inhomogeneities involved.

More complex cycling histories were also conducted in which five successive loading cycles were applied at different temperatures as shown in Figure 10. In this case, the specimen was loaded at higher temperatures following plastic work induced at the RT cycles with an RT–RT–300 °C–600 °C–600 °C loading history. In Figure 10, it can be seen that the load–displacement curves for cycles at higher temperatures show more load serrations than the cycles at RT—evidence of a PLC effect once again. The kink in the curve during the first and third loading cycles is on account of grip relaxation at the specimen–grip interface.

Strains along the line connecting the notch tips were obtained along the least cross section of the specimen between the notches, that is, along the horizontal dashed line in Figure 6(d), as a function of distance along the centerline, with zero denoting the specimen center between the notches. These strain data have been obtained for the peak of each loading cycle, just before unloading begins. At RT (Figure 11(a) and (b)), there is high asymmetry in the strain fields to the left and right sides of the center point, which may be due to geometric inconsistencies induced during the specimen machining process as well as microstructural effects—recall that the average grain size is about 60 μm (30 μm if we consider the annealing twins present). The averaged strain between the left and the right sides of the specimen is also shown in Figure 11.

Continued accumulation of plastic strains occurs over regions where plastic deformation is already higher.[20] This can be observed in Figure 11(b), corresponding to the second cycle, where there is an addition of plastic strain over Figure 11(a), the first cycle, and the same asymmetry in the strain field is still maintained. However, as the temperature is ramped up after unloading of the second RT cycle, the ability of the material to flow is increased, affecting its plastic behavior. With further plastic straining and dynamic aging effects contributing to the straining, the strain field transitions to one with lesser asymmetry (Figure 11(c)–(e)). The averaged response shows continued plastic strain accumulation, which follows the expected trend.

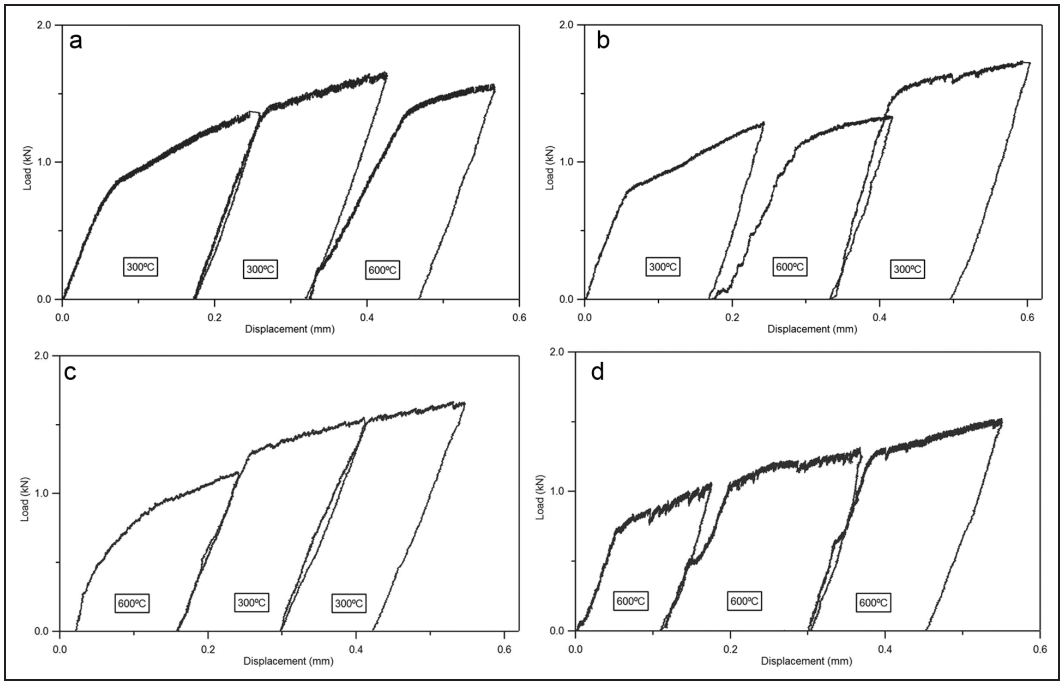

Figure 8. Load–displacement curves from the double-U-notch experiments with thermal cycling: (a) 300 °C–300 °C–600 °C, (b) 300 °C–600 °C–300 °C, (c) 600 °C–300 °C–300 °C, and (d) 600 °C–600 °C–600 °C. When the temperature is changed, there is a change in the elastic modulus and flow stress.

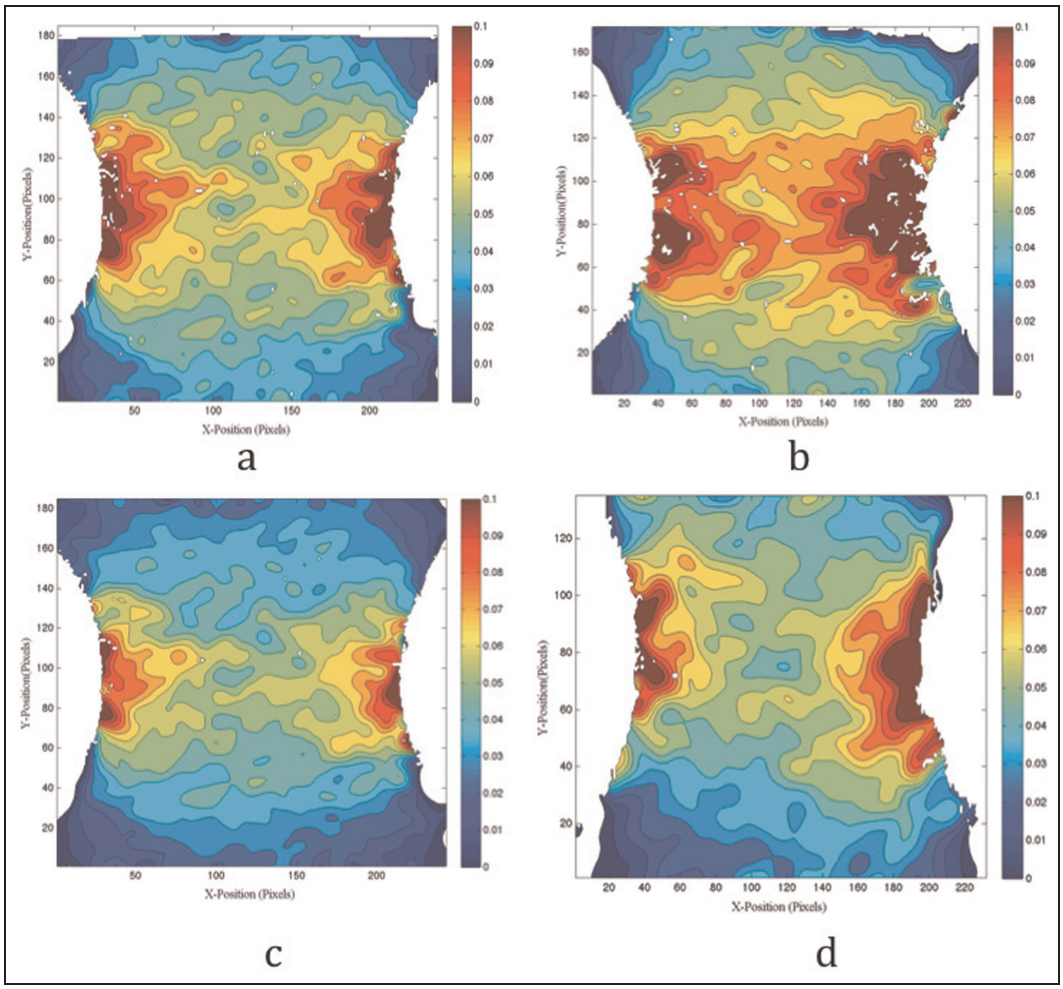

Figure 9. (a) Details of the strain field for an isothermal three loading cycle experiment at 600 °C; (b) strain field for the 300 °C–300 °C–600 °C experiment, showing greater strain accumulation; (c) strain field for the 300 °C–600 °C–300 °C; and (d) strain field for the 600 °C–300 °C–300 °C. It is clear that the strain field is dependent on the temperature history of the material.

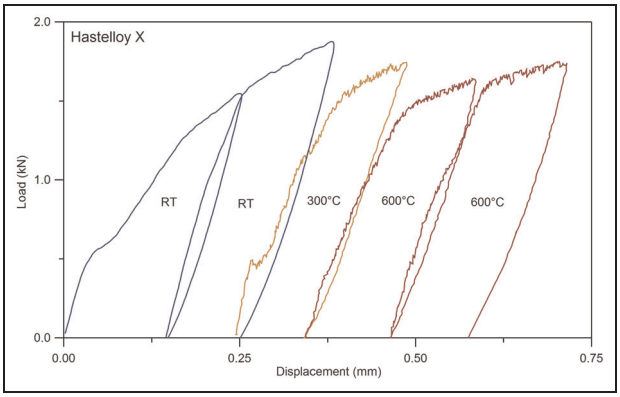

Figure 10. Load–displacement curve for the cyclic loading case. The specimen was subject to five loading cycles—two at room temperature followed by a 300 °C and two 600 °C cycles.

Conclusion

The main objectives of this work were to study the thermomechanical cyclic response of Hastelloy X at elevated temperatures and to understand its behavior in the plastic regime. A consequence of the dynamic strain aging phenomenon was observed to be a CS effect in Hastelloy X, which results in a reduction in flow stress upon reloading at a lower temperature, after pre-loading at a high temperature. The load drop in Hastelloy X is observed to be around 20 MPa (<10% of the flow stress under isothermal conditions). Cyclic loading experiments indicate that the plastic strain accumulated at high temperature influenced by the PLC effect eventually affects the flow stress upon reloading at lower temperatures.

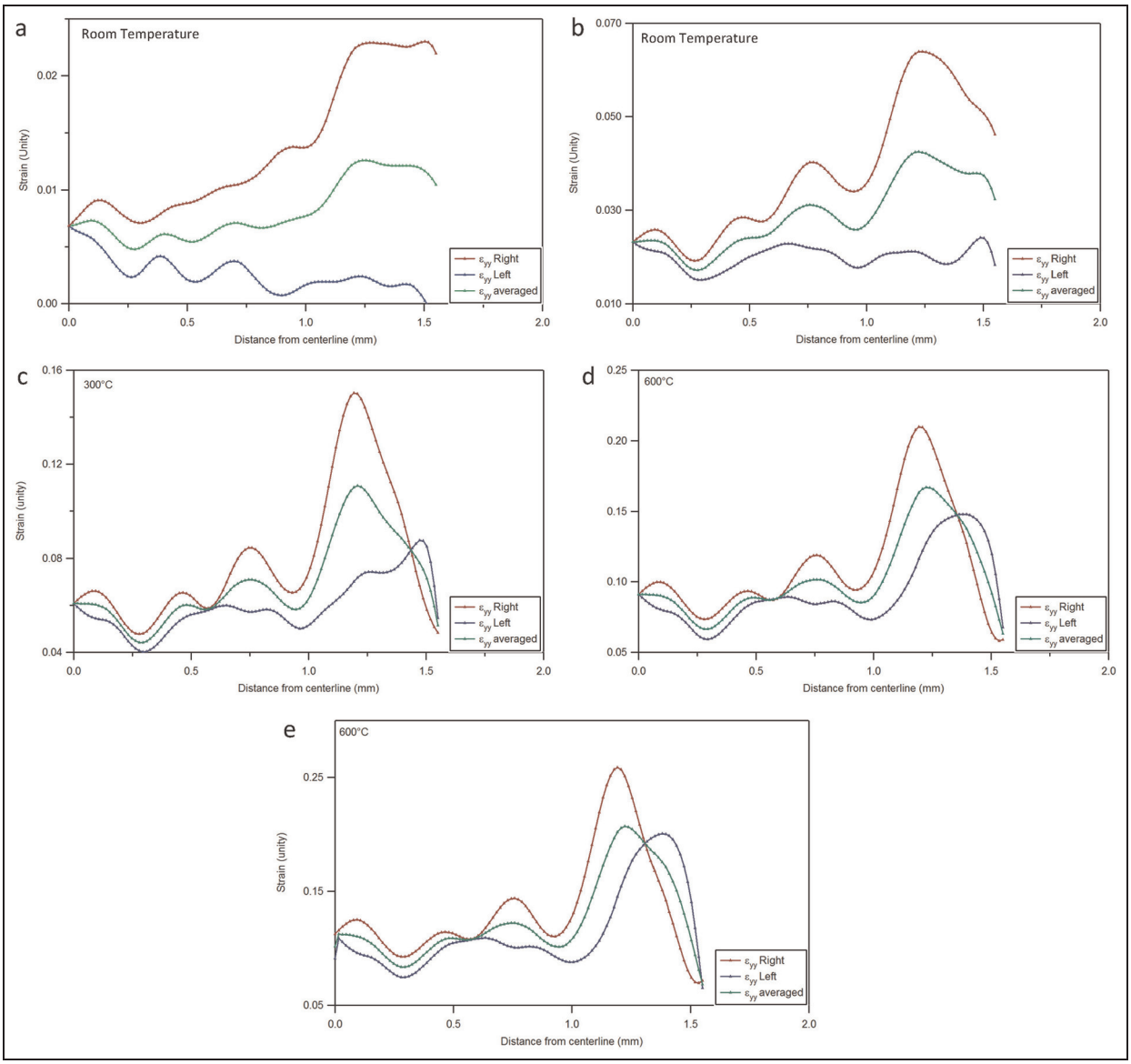

Figure 11. Strain profiles for the cyclic loading experiment at (a) RT, (b) RT, (c) 300 °C, (d) 600 °C, and (e) 600 °C as a function of distance from the centerline.
RT: room temperature.

The effects of cyclic plasticity in the presence of dynamic strain aging and under a biaxial state of stress were also studied. Previous studies showed that the PLC bands initiate around a stress concentration causing further jumps in the strain locally.[9] This work provides some insight into the deformation in Hastelloy X, under biaxial conditions at high temperature. Certain counterintuitive phenomena, such as the establishment of a more symmetric strain state under cyclic loading and larger plastic strains with temperature jump experiments (in comparison to higher temperature isothermal experiments), are possibly explained on the basis of dynamic strain aging.

The results produced from this study have provided an increased knowledge of the effects of dynamic strain aging on the macroscopic plastic deformation and the serrated flow behavior in Hastelloy X. If desired, the study can be extended to higher magnifications where grain level and sub-grain level information can be obtained. Since the DIC method is scale invariant, such higher resolution DIC measurements[15,16] can provide a link between the macroscale response and the microstructural effects in the deformation process.

Declaration of conflicting interests

The authors declare that there is no conflict of interest.

Funding

This study received the support in part of the Midwest Structural Sciences Center (MSSC), which is sponsored by the Air Force Research Laboratory under agreement number FA8650-06-2-3620, and the support of AFOSR award no. FA9550-12-1-0386 (Dr David Stargel is the program monitor).

References

1. United States Department of Defense. *Military handbook—MIL-HDBK-5H: metallic materials and elements for aerospace vehicle structures*. United States Department of Defense, 1998. US Government Department of Defense.
2. Miner RV and Castelli MG. Hardening mechanisms in a dynamic strain aging alloy, HASTELLOY X, during isothermal and thermomechanical cyclic deformation. *Metall Trans A* 1992; 23: 551–561.
3. Jenkins CF and Smith GV. Serrated plastic flow in austenitic stainless steel. *T Metall Soc AIME* 1969; 245: 2149–2156.
4. Sakthivel T, Laha K, Nandagopal M, et al. Effect of temperature and strain rate on serrated flow behaviour of Hastelloy X. *Mat Sci Eng A: Struct* 2012; 534: 580–587.
5. Swaminathan B, Abuzaid W, Lambros J, et al. Investigation of Portevin–Le Chatelier effect at elevated temperatures in HASTELLOY X using digital image correlation. *Int J Plasticity* (submitted).
6. Cottrell AH and Stokes RJ. Effects of temperature on the plastic properties of aluminium crystals. *Proc R Soc Lon Ser: A Mat* 1955; 233: 17–34.
7. Kubin LP and Estrin Y. Evolution of dislocation densities and the critical conditions for the Portevin–Le Chatelier effect. *Acta Metall Mater* 1990; 38: 697–708.
8. Kubin LP and Estrin Y. The critical conditions for jerky flow. Discussion and application to CuMn solid solutions. *Phys Status Solidi B* 1992; 172: 173–185.
9. Tong W, Xuan X and Yao H. On the interaction of material heterogeneity and geometric discontinuity in serrated plastic flows. In: *3rd International conference on heterogeneous material mechanics*, Shanghai, China, 22–26 May 2011, pp.178–185. Lancaster, PA, USA: DEStech Publications Inc.
10. Turner JL and Russell SS. Application of digital image analysis to strain measurement at elevated temperature. *Strain* 1990; 26: 55–59.
11. Coburn D and Slevin J. Digital correlation system for nondestructive testing of thermally stressed ceramics. *Appl Optics* 1995; 34: 5977–5986.
12. Lyons JS, Liu J and Sutton MA. High-temperature deformation measurements using digital-image correlation. *Exp Mech* 1996; 36: 64–70.
13. Pan B, Wu D and Xia Y. High-temperature deformation field measurement by combining transient aerodynamic heating simulation system and reliability-guided digital image correlation. *Opt Laser Eng* 2010; 48: 841–848.
14. Benallal A, Berstad T, Børvik T, et al. An experimental and numerical investigation of the behaviour of AA5083 aluminium alloy in presence of the Portevin–Le Chatelier effect. *Int J Plasticity* 2008; 24: 1916–1945.
15. Carroll JD, Abuzaid W, Lambros J, et al. On the interactions between strain accumulation, microstructure, and fatigue crack behavior. *Int J Fracture* 2013; 180: 223–241.
16. Abuzaid W, Sehitoglu H and Lambros J. Plastic strain localization and fatigue micro-crack formation in Hastelloy X. *Mat Sci Eng A: Struct* 2013; 561, 507–519.
17. Sutton M, Wolters W, Peters W, et al. Determination of displacements using an improved digital correlation method. *Image Vision Comput* 1983; 1: 133–139.
18. Sobotka JC and Dodds RH. Extension of generalized plasticity model for thermo-cyclic loading. *J Eng Mater: T ASME*, in press.
19. Abuzaid WZ, Sangid MD, Carroll JD, et al. Slip transfer and plastic strain accumulation across grain boundaries in Hastelloy X. *J Mech Phys Solids* 2012; 60: 1201–1220.
20. Basinski Z. Forest hardening in face centred cubic metals. *Scripta Metall* 1974; 8: 1301–1307.